Attentional amplification of neural codes for number independent of other quantities along the dorsal visual stream

Elisa Castaldi[1]*, Manuela Piazza[2], Stanislas Dehaene[1], Alexandre Vignaud[3], Evelyn Eger[1]

[1] Cognitive Neuroimaging Unit, CEA DRF/JOLIOT, INSERM, Université Paris-Sud, Université Paris-Saclay, NeuroSpin center, France

[2] Center for Mind/Brain Sciences, University of Trento, Italy

[3] UNIRS, CEA DRF/JOLIOT, Université Paris-Saclay, NeuroSpin center, France

*Corresponding author

E-mail: elisa.castaldi@gmail.com

Major Subject Area(s): Neuroscience

Abstract

Humans and other animals base important decisions on estimates of number, and intraparietal cortex is thought to provide a crucial substrate of this ability. However, it remains debated whether an independent neuronal processing mechanism underlies this “number sense”, or whether number is instead judged indirectly on the basis of other quantitative features. We performed high-resolution 7 Tesla fMRI while adult human volunteers attended either to the numerosity or to an orthogonal dimension (average item size) of visual dot arrays. Numerosity explained a significant amount of variance in activation patterns, above and beyond non-numerical dimensions. Its representation was progressively enhanced along the dorsal visual pathway and was selectively amplified by attention when task relevant. These results reveal a dedicated extraction mechanism for numerosity that operates independently of other quantitative dimensions of the stimuli, and suggest that later stages along the dorsal stream are most important for the explicit manipulation of numerical quantity.

Introduction

One largely debated theme in cognitive neuroscience is how the human brain developed the ability to perform mathematics. While mathematical skills certainly rely on the interplay of a wide range of cognitive functions (De Smedt et al., 2013; Fias, 2016; Iuculano and Menon, 2018), an influential theory in the field proposes that a necessary prerequisite to develop such a sophisticated uniquely human ability resides in the 'number sense' (Dehaene, 1997). This is a phylogenetically ancient competence that enables humans and other animals to assess and mentally manipulate the approximate number of objects in sets. In humans the precision of the number sense (or 'numerical acuity', typically measured by visual number discrimination) sharpens with age and with the acquisition of formal mathematical education (Piazza et al., 2013), and correlates with arithmetical skills throughout the life-span (Halberda et al., 2008; Libertus et al., 2011, 2013; Chen and Li, 2014; Anobile et al., 2016a, 2018). Deviations from the typical developmental trend of numerical acuity can be a symptom of developmental dyscalculia (Piazza et al., 2010), a neurodevelopmental disorder that causes specific mathematical learning difficulties.

The neural substrate subtending this sense of numerical quantity is thought to be shared across species and has been linked to a network of areas in the frontal and parietal cortices sensitive to changes in numerosity since very early in life (Izard et al., 2008; Hyde and Spelke, 2011; see for reviews: Cantlon, 2012; de Hevia et al., 2017). In these areas electrophysiological recordings in monkeys identified single neurons tuned to specific numerosities of visual arrays (Nieder et al., 2002; Nieder and Miller, 2004; Roitman et al., 2007; Nieder, 2016) and fMRI studies in humans found activation in these areas to be modulated during quantity perception as well as during calculation (for reviews see: Arsalidou and Taylor, 2011; Eger, 2016; Piazza and Eger, 2016). While the first imaging studies in humans were limited by the low spatial resolution and univariate subtraction-based analyses, fMRI adaptation and multivariate pattern analysis methods provide higher sensitivity to finer-scale activity differences (Kourtzi and Grill-Spector, 2005; Norman et al., 2006; Tong and Pratte, 2012). These methods allowed researchers to study the representation of individual numbers by recording the distance-dependent signal release from adaptation (Piazza et al., 2004), or reading out patterns of number-related activity across multiple voxels of the frontal and parietal cortex (Eger et al., 2009). Moreover, population-receptive field mapping (pRF) methods identified individual locations tuned to specific numerosities arranged in spatially organized maps in the parietal cortex (Harvey et al., 2013).

While these earlier findings mostly pointed at the key role of parietal and frontal areas in numerical representation, some recent studies found that it is possible to decode the number of items seen by the subjects from the fMRI activity patterns in early visual areas (Bulthé et al., 2014; Eger et al., 2015; Bulthé et al., 2015; DeWind et al., 2018, but see Castaldi et al., 2016). Moreover, spatially organized numerosity maps were recently claimed to extend to the occipital cortex (Harvey and Dumoulin, 2017a) and early ERP components compatible with generators in early visual areas responded to variations in the numerosity of visual arrays (Park et al., 2015; Fornaciai et al., 2017; Fornaciai and Park, 2017).

Several properties characterizing numerosity perception, such as being ratio-dependent (Weber's law) and being susceptible to adaptation, led some authors to suggest that number is a "primary" visual property of the image that is directly perceived through specialized and dedicated mechanisms (Burr and Ross, 2008; Ross, 2010; Anobile et al., 2016b). However, in spite of dedicated efforts on modeling the extraction of numerosity from the visual image (Dehaene and Changeux, 1993; Verguts and Fias, 2004; Dakin et al., 2011; Stoianov and Zorzi, 2012; Morgan et al., 2014), the detailed neural processing mechanisms used by the brain to arrive at a representation of numerosity from the visual input remain little understood, and much less understood than the ones for other basic visual features such as orientation, colour, motion, etc. Numerosity is a notoriously difficult feature to study since changes in numerosity tend to be associated with changes in other quantitative features of the sets during natural viewing conditions (e.g., more items tend to occupy a larger area, or be spaced more densely), and it appears impossible to control for all of these associated quantities at the same time. For this reason, in spite of a large body of behavioural and neuroscientific work on this topic, it still remains debated whether the available evidence supports a dedicated neuronal processing mechanism for numerosity. Some have argued instead that numerosity might be judged indirectly by weighing a combination of other, non-numerical, quantitative features of the stimuli (Gebuis and Reynvoet, 2012; Gebuis et al., 2014; Leibovich et al., 2016). For example, numerosity can be mathematically defined as the product of density (number of items per unit of area) by field area; or by the total surface area divided by mean item size. Thus, decisions on numerical quantity could be taken merely indirectly, on the basis of representations of these non-numerical properties, without numerosity being encoded directly by perceptual systems.

While this possibility is interesting, several behavioural findings argue against it: (1) the discrimination of numerosity and of one often correlated non-numerical feature (item density) follow different psychophysical laws (Anobile et al., 2016b), and (2) at least for relatively small numbers of not too densely spaced items, perceptual thresholds for numerosity discrimination are typically much smaller than the ones predicted from the thresholds for

density and field area together (Cicchini et al., 2016), making it unlikely that estimates of numerosity are based on the latter. For what concerns the neuronal level, a few recent studies have started to directly quantify the effects of non-numerical dimensions of non-symbolic numerical stimuli (e.g. Park et al., 2015; Fornaciai et al., 2017; Harvey and Dumoulin, 2017b; Fornaciai and Park, 2018; DeWind et al., 2018). Those studies found that activity in earlier (occipital) or later (parietal) brain regions appeared to be linked to the numerical content of sets after taking into account effects of certain non-numerical dimensions. However, they mostly only considered the effect of one non-numerical variable at the time and compare it to that of number, without taking into account effects explained by all relevant non-numerical dimensions together. Thus, it still remains unclear to what extent activity evoked by non-symbolic numerical stimuli within early and later regions can be explained by a mechanism that encodes numerosity in itself, or by the ensemble of responses to the different non-numerical dimensions of the stimuli.

Here, we implement a new approach to separate brain signals related to numerical and non-numerical quantities and test for a dedicated neuronal mechanism for extracting the numerosity of visual sets. We reasoned that the following signatures would advocate for the existence of such a mechanism:

First, information on numerosity should be detectable in activity patterns after multiple important non-numerical quantities are simultaneously (and not only individually) taken into account. Second, and importantly, this information should be specifically amplified depending on whether the numerical dimension of the stimuli is task relevant. If numerosity is an independently encoded perceptual feature, it should be possible to selectively enhance its brain representation by attention, as it has been previously shown for other task-relevant primary features, such as orientation, contrast, color, direction etc. (Jehee et al., 2011; Ester et al., 2016). In other words, tasks involving selective attention to number should enhance the information about numerosity in the relevant brain areas, without affecting the level of information on associated non-numerical dimensions. In fact, we propose that the presence of such attentional amplification is a key criterion in order to identify which brain areas explicitly encode numerosity.

On the contrary, if activity patterns could be entirely accounted for by the combination of responses to multiple non-numerical dimensions of the stimuli, no information specifically related to number should be found in the patterns of activity once accounting for the other (non-numerical) dimensions simultaneously. Furthermore, if numerosity was not directly encoded but only indirectly inferred from percepts of non-numerical properties, attentional

enhancement should not occur for signals related to numerosity, but if anything, only for other properties (e.g., density and field area) that can jointly define it.

To test these predictions, we created a novel stimulus space to disentangle the contribution of numerical and non-numerical dimensions to brain activity patterns, and designed a task where attention is selectively directed towards either of two orthogonal quantitative dimensions of the visual array (number or item size). We exploited the enhanced sensitivity achieved by fMRI at ultra-high field (7 Tesla) and specific multivariate pattern analyses to simultaneously model and separate the contributions of the different numerical and non-numerical quantities to fine-scale activity patterns within multiple regions defined by a probabilistic atlas based on visual topography.

Results

We scanned twenty healthy adult volunteers while they performed two tasks on arrays of dots varying orthogonally in numerosity (6, 10, or 17 items), average item size (0.04, 0.07, or 0.12 visual square degrees - vd^2) and total field area (44 or 20 vd^2) (Fig 1A). Participants alternated between a “number” and a “size” task in different blocks: during the “number” blocks they had to direct attention to the numerosity of each sample stimulus and keep it in memory for comparison with an occasionally following match stimulus, while during “size” blocks they performed the equivalent task on the average item size of the arrays (Fig 1B). When a match stimulus appeared (indicated by a change in color of the fixation point), participants had to decide whether the match stimulus was larger or smaller on the attended dimension than the previous sample held in memory and to respond by button press.

Behavioral performance and univariate fMRI activation effects

Response accuracies for comparison of match stimuli were overall high and not significantly different across tasks (86% for the number task and 85% for the average size task, $t(19) = 0.46$, $p = 0.65$), suggesting that subjects attended to the correct stimulus dimension and the difficulty was on average successfully matched across tasks (Fig 2A).

We started the analysis of the functional imaging data by evaluating overall regional activation effects during both tasks. Surface-based random-effects group analysis identified similar bilateral activations in the occipito-parietal and frontal cortex during both tasks for

sample stimuli against the implicit baseline (Fig 2B and 2C, thresholded at p<0.001 uncorrected). To localize activity in relation to the major sulci and gyri, an anatomical brain parcellation based on the Destrieux Atlas (Fischl, 2004) was superimposed onto the activity maps. In both tasks the activity covered a wide occipito-parietal area starting from the superior occipital and transverse occipital sulci and extending throughout the intraparietal sulcus up to the post-central sulcus. The frontal activity mainly covered the superior frontal gyrus. The direct contrast of sample stimulus-related activity during the number versus the size task revealed no area with significantly stronger activation for either of the two, despite the uncorrected significance threshold (Fig 2D). Altogether, these results suggest that task difficulty was successfully matched and that under these conditions attending to different quantitative dimensions leads to equivalent overall activation of the brain regions involved in the task. Differences in overall activation level can therefore not confound the following more specific results on the within-dimension discriminability of quantitative features.

Multivariate fMRI Pattern Analyses

Read-out of sample numerosity is modulated by task

Given that the whole brain univariate contrasts had confirmed equivalent activations across the two tasks, we further investigated, using multivariate classification, what was the degree of discriminability of activity patterns evoked by different sample numerosities across different regions of the dorsal visual stream and during the number and size task. In each subject we identified several regions of interest (ROIs) derived from a surface-based probabilistic atlas based on visual topography (Wang et al., 2015, Fig 3A). Within each region, we used an equivalent number of most activated voxels (in the orthogonal contrast 'all sample stimuli > baseline') to train and test multivariate classifiers to discriminate between numerosities for each task. Fig 3B shows the across-subject overlap map for the included voxels which mainly highlight the foveal portion of the different ROIs, in line with the central presentation of the dot arrays. We first compared decoding accuracies in three large regions corresponding to early, intermediate and higher level areas (including areas from V1 to V3, from V3AB to V7 and from IPS1 to IPS5, respectively). Then, to track the presence of information discriminative of numerosity across the dorsal visual stream more in detail, we further compared the classification accuracies across seven contiguous ROIs from V1 up to IPS345. Fig 3C shows the performance of the classifiers trained to discriminate between different numerosities as a function of task. Overall, the presented sample numerosity could be decoded in all the ROIs and during both the number and size task, however with important differences. When explicitly attending to numerosity, the classification accuracy

gradually increased across the dorsal stream (starting to be enhanced from intermediate areas, specifically from V3AB on), and was highest in parietal areas. During the size task, when attention was not explicitly directed towards the numerical aspect of the stimuli, the different numerosities were still decodable, however the classification accuracies were reduced in intermediate and higher regions, while they remained almost unchanged in early visual areas (specifically in V1, V2 and V3).

The task-driven modulation of decoding accuracies across the three major ROIs is confirmed by a significant interaction between ROI and task ($F(2,38) = 9.81$, $p = 0.0004$). For the number task, the classification accuracy progressively increased from the early visual areas (slightly above 60%) to intermediate and higher level regions where it reached almost 70% correct. Post-hoc tests showed that the classification accuracy increase in intermediate and higher areas with respect to early areas was very close to or clearly significant ($p = 0.075$ and $p = 0.028$ respectively). During the size task, the classification accuracy in the intermediate and higher regions dropped down to 61% and 60% respectively (yet remaining highly significantly above chance in both cases, see p-values in Table 1 in Supplementary materials). The change in classification accuracy across tasks was highly significant both for the intermediate and higher areas ($p = 0.001$ and $p = 0.00001$). On the other hand, the classification accuracy in the early visual areas remained nearly constant (62%) and was not significantly modulated by task ($p = 0.5$).

The significant interaction between ROI and task was confirmed when testing the seven individual regions ($F(6,114) = 7.17$, $p = 0.000002$). Although the post-hoc tests did not show significant differences in classification accuracies across individual ROIs, for the number task the decoding accuracies progressively increased across the visual hierarchy and varied from slightly above 60% in the primary visual areas (V1 = 62%, V2 = 62%, V3 = 61%) up to almost 70% in the intermediate and higher ROIs (V3AB = 64%, V7 = 65%; IPS12 = 67%, IPS345 = 67%). During the size task, decoding accuracies were much reduced in intermediate and higher regions (V3AB=58%, V7=58%; IPS12=59%, IPS345=58%, yet still significantly above chance in all ROIs, see p-values in Table 1 in Supplementary materials), while they remained almost unchanged in the primary visual areas (V1 = 61%, V2 = 62%, V3 = 60%). Accordingly, the post-hoc tests indicated that the classification accuracy in individual regions significantly changed across tasks only from V3AB on (V1: $p = 0.28$; V2: $p = 0.83$; V3: $p = 0.55$; V3AB $p = 0.0002$; V7: $p = 0.00003$; IPS12: $p = 0.00001$; IPS345: $p = 0.00005$).

In sum, multivariate classification analyses revealed that the sample numerosity presented could be read out from brain activity patterns in all ROIs tested during both tasks, although accuracy was enhanced in mid-to-higher level but not in earlier regions when

number was the attended feature. However, since in this analysis activations for all sample stimuli for a given numerosity were pooled together, the decoding performance obtained could still be partly driven by features other than numerosity per se.

Multiple regression RSA to disentangle the contributions of quantitative dimensions

As a critical test of whether the representations of numerical and non-numerical features of the stimuli could be dissociated across the dorsal visual stream, we performed Representational Similarity Analysis (RSA, Kriegeskorte, 2008; Kriegeskorte and Kievit, 2013) which, unlike classification-based decoding, allows to assess the effect of multiple quantitative dimensions on activity patterns simultaneously. For each ROI and task, we obtained a neural representational dissimilarity matrix (neural RDM, Fig 4A) by computing the correlation distance between activation patterns for each possible pair of conditions. We then applied multiple regression analysis to test in how far the fMRI pattern dissimilarity structure could be explained by multiple predictor matrices reflecting the stimuli's dissimilarity along several important quantitative dimensions: numerosity, average item size, total field area, total surface area and density (Fig 4B). Of note, our design orthogonally manipulating numerosity, average item size and total field area ensured that numerosity was also partly decorrelated from density and total surface area (as shown by the correlation values in the Predictor Correlation matrix, Fig 4B), allowing for a good dissociation between stimulus descriptors. By using a multiple regression approach we capitalize on the fact that the resulting beta weights reflect only the part of the variance that each one of these stimulus descriptors uniquely explained in the pattern of activity of a given ROI on top of the contribution of all the others. Indeed, by entering numerical and non-numerical dimensions together into a multiple regression, a significantly above zero beta for number would imply that the numerical information is contributing to the pattern of activity within a given ROI, over and above the contribution of the other non-numerical quantitative dimensions.

Fig 5 displays the results of the estimated beta weights for various ROIs separately for the number (Fig 4A) and size tasks (Fig 4B). Beta weights for the effect of number independent of the other dimensions (black triangles) were generally positive and progressively explained the activity patterns better when proceeding from lower to higher-level regions when task relevant. The evolution of the numerical information across the visual stream was attenuated during the size task, yet betas remained significantly above zero in all regions (see p-values in Table 2 in supplementary material). Beta weights for the non-numerical dimensions (other

shapes in Fig 4) were pronounced predominantly in the earlier visual areas and, importantly, they appeared to be not clearly affected by task.

Quantitative dimensions are modulated by task across ROIs to different extent

To statistically test for differential modulation of the contribution of the different quantitative dimensions to activation patterns, beta weights were analyzed with repeated measure ANOVAs with ROI, task and dimension as factors. As for the classification analysis, we first focused on the three large regions corresponding to early, intermediate and higher-level areas and then further on individual ROIs from V1 up to IPS345.

The significant triple interaction between ROI, task and dimension confirmed that the beta weights estimated for the different dimensions were differently affected by task across ROIs (for the three large regions: $F(4.42,80.40) = 3.32$, $p = 0.01$; for the individual regions: $F(24,456) = 3.06$, $p = 0.000002$). To identify which dimension was maximally driving this effect, we quantified the changes in beta weights across ROIs and tasks for each dimension separately.

Effects of the numerical dimension

Beta values for number were the only ones showing a significant interaction between ROI and task, when comparing the three large subdivisions across the visual stream ($F(1.35,25.61) = 5.97$, $p = 0.015$). During the number task, betas for number were higher in intermediate and higher-level areas with respect to early visual areas (although only the former comparison was significant, $p=0.04$). During the size task the betas for number were significantly lower (significant difference across tasks in early: $p = 0.007$; intermediate: $p = 0.000001$; higher areas: $p = 0.00001$) and not different across regions.

When focusing on the seven individual ROIs, the interaction between ROI and task was significant ($F(2.04,38.83) = 5.29$, $p= 0.009$). Although post-hoc tests did not identify significant differences across ROIs, linear regression showed that the increase in beta weights for number across the dorsal visual stream was significant during the number task only ($F(1,5) = 14.23$, $p = 0.01$, $R^2 = 0.74$), while during the size task betas for number were much more homogenous across ROIs ($F(1,5)=2.37$, $p = 0.18$, $R^2 = 0.32$). Indeed the difference in beta weights between the number and size task was only minor or not significant in V1 and V2, more pronounced in V3, and highly significant from V3AB on

(difference across tasks: V1: p = 0.025; V2: p = 0.13; V3: p = 0.001; V3AB p = 0.000001; V7: p = 0.000008; IPS12: p = 0.000001; IPS345: p = 0.000112).

Effects of the non-numerical dimensions

Different from number, beta weights estimated for the non-numerical dimensions were not modulated by task (no significant interaction between ROIs and task, no significant main effect of task) for any of the dimensions.

Independent of the task, total field area best explained activity patterns in early visual areas, while its contribution was reduced when proceeding through intermediate to higher-level areas (significant main effect of ROIs: F(1.22,23.29) = 35.24, p = 0.000002; significant differences in beta weights between primary and intermediate or higher-level ROIs: p = 0.000155, p = 0.000008, respectively). Beta values were highly significantly modulated also across the different individual ROIs (main effect of ROIs: F(2.11,40.11) = 32.27, $p < 10^{-5}$). Indeed, activity patterns in V1, V2 and V3 were explained equally well by total field area and better than intermediate and higher regions, starting from V3AB on (all p < 0.01 at least).

Total surface area also most strongly modulated pattern dissimilarity in early visual areas. The significant main effect of ROI (F(1.4,27.63) = 16.61, p = 0.000078) and the following post-hoc tests showed that beta values for this dimension in the early visual areas were significantly higher than those estimated for the intermediate (p = 0.000475) and higher-level (p = 0.000943) ROIs, independent of the task. Beta weights for total surface area were comparable in V1, V2 and V3 (no significant difference across these ROIs) and significantly higher than those of the others ROIs starting from V3AB/V7 on (significant main effect of ROI: F(3.13,59.41) = 13.27, p = 0.000001, comparisons across regions: all p < 0.01 at least).

Density modulated early visual areas during the number task and both earlier and higher-level areas during the size task. The main effect of ROI was significant (F(1.41,26.72) = 4.05, p = 0.04), but additional post-hoc tests did not reveal any significant difference across the three large ROIs. Also at the level of individual regions the main effect of ROI was significant (F(2.55,48.54) = 4.15, p = 0.01) and the strongest difference across ROIs emerged when comparing the lowest beta weights estimated in V3AB with those obtained in V1 (p = 0.003) and V7, IPS12 and IPS345 (p = 0.03, p = 0.01, p = 0.002).

Surprisingly, effects due to average item size could not be detected in any of the ROIs tested.

In sum, while early visual areas contained independent information on multiple quantitative properties of which some explained more variance than numerosity, all regions were modulated to some extent by numerical distance over and above what was explainable by the non-numerical dimensions. Moreover, importantly, explicitly directing attention to number did enhance the representation of numerical information and did so selectively, without altering the representations of non-numerical quantities. Finally, although present starting from the earliest stages of visual analysis, the numerical information at this level was only to a minor extent modulated by task and the greatest contribution to explicit manipulation of numerical quantity was found in intermediate and higher-level regions.

Discussion

Our work exploited the enhanced spatial resolution provided by ultra-high field fMRI to reveal how the human brain represents multiple quantitative dimensions of non-symbolic numerical stimuli. Furthermore, we tested whether and at what cortical level the numerical information can be represented and specifically modulated by attention independently of non-numerical visual properties of the image.

At the level of overall regional activity, attending to the numerosity or to the average size of the dots in the array recruited largely overlapping occipital and parietal areas, as also previously observed for perception and comparison of different types of quantities (Pinel et al., 2004; Dormal and Pesenti, 2009; Borghesani et al., 2018; for a meta-analysis on other non-numerical representations see: Sokolowski et al., 2017). Only multivariate pattern analysis could detect differences in the way information along the different dimensions was encoded as a function of task in our study. Importantly, the equal percentage of correct responses across tasks ensured that the differences detected could not be attributed to an overall unspecific difference in task difficulty.

Multivariate decoding analyses showed that the sample numerosity presented could be read out from brain activity all along the visual stream, however with important differences across regions. When explicitly attended, the numerical information could be read out with gradually higher accuracy following an occipital-parietal gradient, up to a maximum level in the parietal cortices. The effect of attention strongly affected the accuracy of the numerical discrimination in intermediate and higher regions while leaving the accuracy in the early visual areas unaffected. The successful read-out of information related to numerosity from parietal cortices in the current experiment contrasts with some previous studies where fMRI signals discriminative of numerosity information could not be detected in the parietal regions (DeWind et al., 2018; Fornaciai and Park, 2018). Differences in paradigms and sensitivity of the scanners used may account for this discrepancy. Most crucially, in those studies, participants were shown with different numerosities and the task required detecting changes in the colour of the dots. Thus, participants' attention may have not been directed to the numerosity of the visual arrays in that case, and the numerical information may have been reduced when focussing on the dots' colour, similarly to what was observed for the size task in the current experiment. Although in the present study we could still read out numerical information even when it was irrelevant for the task, this signal may have remained undetected by less sensitive MRI scanners.

In the current study the number presented could be decoded from the earliest stages of visual processing. However, since this analysis collapsed across the non-numerical dimensions of our stimulus set it is unclear whether the information underlying successful decoding was strictly numerical, especially in earlier regions. Some previous studies have dealt with the problem of correlations between numerical and non-numerical stimulus dimensions by controlling for non-numerical features one at the time and testing for fMRI adaptation effects, or replicability of decoding performance or layouts across conditions where individual non-numerical features where controlled for (Piazza et al., 2004; Eger et al., 2009; Harvey et al., 2013; Harvey and Dumoulin, 2017a; DeWind et al., 2018). When the effects of non-numerical dimensions were measured directly, this was done in some studies by computing the explained variance or classification performance for each feature in isolation and comparing it to the one for number (Harvey and Dumoulin, 2017b; Cavdaroglu and Knops, 2018), leaving open the degree to which the simultaneous contribution of several non-numerical dimensions could account for the findings (Gebuis et al., 2014). Some other previous studies have taken a different approach, by modelling jointly the effects of numerosity and two non-numerical dimensions (termed “size in area” and “spacing”) which were designed to be orthogonal to numerosity but do not necessarily constitute natural, perceptually relevant feature dimensions, but rather mathematically defined constructs (DeWind et al., 2015; Park et al., 2015; DeWind et al., 2018; Fornaciai and Park, 2018). This design also allowed the authors to estimate, from the combined beta weights of numerosity and the mentioned two orthogonal dimensions, which feature represented by different directions in their stimulus space most accounted for the effects in a given ERP component or brain area. However, brain signals can reflect a combination of responses to multiple quantitative dimensions, and this approach does not permit to distinguish, for example, a modulation by numerosity from two independent modulations by field area and density.

In our study, on the contrary, we separated the contributions of numerical and non-numerical stimulus dimensions by applying multiple regression to representational distance matrices which allowed us to test for the extent to which numerosity could explain the pattern of activity while taking into account simultaneously the variability explained by several important natural non-numerical features. Indeed estimating significantly above zero beta values for number implies that information about numerosity is present in the pattern of activity over and above the contributions of all the non-numerical features. We found that information specific to number was detectable beyond the information of the other dimensions, and that the numerical information was gradually enhanced when progressing along the visual stream when explicitly task relevant, and much more weakly represented, although still detectable, when not task-relevant. Importantly, the level of information on other

quantitative but non-numerical properties of the image, such as total field area, total surface area and density, although reliably detected, especially in earlier brain regions, was not altered when explicitly attending to the numerical quantity. The presence of separable contributions of the representations of numerical and non-numerical dimensions in activation patterns together with the selective attentional modulation of the numerical information provides strong evidence for a specific neuronal extraction mechanism dedicated to the property number. The fact that such specifically numerical information is found from early stages of the cortical hierarchy on, and that attentional modulation does not affect associated non-numerical quantities makes it unlikely that numerical judgements would only be made indirectly on the basis of different non-numerical features.

The enhancement of numerical information in activation patterns found here when number was the relevant stimulus dimension is extending a growing body of work on the neuronal correlates of feature-based attention. Neurophysiological studies have shown that attention to basic visual features either increases the gain or sharpens responses of neuronal populations preferentially responsive to these features in different visual areas (e.g. Treue and Trujillo, 1999; McAdams and Maunsell, 2000; Reynolds et al., 2000; Martinez-Trujillo and Treue, 2004; David et al., 2008, see also: Carrasco, 2011 for a review). Correspondingly, fMRI decoding studies have found that directing attention to one feature dimension such as orientation, motion direction or color or to particular values within one given dimension improves the read-out of these features from brain activity in early sensory regions (Kamitani and Tong, 2005, 2006; Serences and Boynton, 2007; Jehee et al., 2011) but in some cases also in higher-level areas (Liu et al., 2011; Ester et al., 2016). According to one influential account, higher-level fronto-parietal areas such as the lateral intraparietal area (LIP) implement spatial “priority maps” in which the level of activity at individual locations depends jointly on the different features of objects at these locations as well as on top-down factors such as their task relevance, associated reward, etc (Itti and Koch, 2001; Thompson and Bichot, 2005; Gottlieb, 2007; Sapountzis et al., 2018). Independent of spatial priority, LIP neurons have also been found to represent higher-level factors such as learned category membership and other non-spatial information (Freedman and Assad, 2009) and to flexibly switch between encoding of different visual features, such as color or motion, depending on the task (Toth and Assad, 2002; Ibos and Freedman, 2014). The idea of a role for intraparietal areas as mere “priority maps” or reflecting entirely flexible encoding of information on task-relevant features (without intrinsic selectivity) can insufficiently account for our results, since it would predict an equivalent amplification of the representation of average size when this is the attended feature instead of number. This is not what we observed. Our results are thus more compatible with an enhancement of the responses of

neuronal populations with intrinsic selectivity to the feature numerosity in these areas (comparable to the one observed for other features in lower-level visual regions).

While the existence of individual neurons tuned to different numbers of items in intraparietal cortex is well established (Nieder and Miller, 2004; Roitman et al., 2007), the only electrophysiological study that recorded from neurons in the ventral intraparietal (VIP) cortex in macaque monkeys under changing task conditions (Viswanathan and Nieder, 2015) found that neurons encoded numerosity to the same extent, regardless of whether the task required to attend to the number or the color of the items. This differs from our results which show a clear attentional amplification of numerosity information. Given that the human IPS 1-5 investigated in the current work is usually considered to be the equivalent of the macaque LIP/VIP complex (Kastner et al., 2017), the difference between results may be due to a difference across species, but differences in paradigms and in the nature of the signal recorded in the two studies make it difficult to directly relate the two findings. For example, monkeys were trained initially with the color match to sample task, then re-trained to respond to number, thus implying comparisons across an extended time period and different context, whereas our participants switched between the two tasks within the same scanning session. In addition, it is possible that the color task with a single color per stimulus and a small number of highly distinguishable alternatives placed lower demands on attentional load compared to our average size task, therefore leaving number processing unaltered. Nevertheless, as a common denominator both studies agree on pointing to some degree of spontaneous encoding of numerosity in intraparietal areas under conditions of attention to an orthogonal stimulus dimension.

The gradual enhancement of numerosity information observed by us in the number task when progressing along the dorsal visual stream is compatible with a multi-stage process of the extraction of numerosity where attention may operate at multiple levels over which attentional enhancements accumulate. If numerosity information can be retrieved from multiple levels of the cortical hierarchy, this does not need to imply that this features is encoded by individual neurons at all these levels, but it may be detectable by multivariate methods even if it existed only in distributed form across the population of neurons. As one speculative interpretation, the numerical information read out from early visual areas could reflect a location map (Dehaene and Changeux, 1993), or the process of object segmentation where different individual items start to be separately represented, but this representation may not yet be in a form that is most easily read out for numerical discrimination. Higher areas may progressively transform and concentrate the initially distributed information onto individual neurons, which most likely constitute the base on which we operate when comparing numbers. This interpretation is in line with a recent study

showing that although different numerosities could be discriminated based on the pattern of activity in early visual areas and parietal cortex, the behavioral precision of numerical discrimination was correlated with the decoding accuracy only in the latter region (Lasne et al., 2018).

A surprising result of the current experiment is that we could not find information about average item size in the pattern of activity in any of the regions examined, even though this feature's perceptual discriminability was equated with the one of numerosity. This suggests that the neural mechanisms supporting average size representation may differ from those engaged during single object size analysis which has been shown to overlap partly with numerosity maps in parietal regions (Harvey et al., 2015). Mechanisms for average size perception, and in general for ensemble statistics are still unclear. It has been previously suggested that average item size perception, like density perception, may rely on texture processing mechanisms rather than individual item identification (Im and Halberda, 2013). Various regions along the ventral visual stream have been implicated in texture perception. In particular, adaptation studies have identified recovery of fMRI signal in the medial part of the posterior collateral sulcus that was selective for texture as opposed to color or shape of 3D irregular objects (Cavina-Pratesi et al., 2010) and the parahippocampal place area (PPA) showed equal release from adaptation for object ensemble and surface textures, suggesting that ensembles and textures are processed similarly (Cant and Xu, 2012). It is possible that average size is also represented in the ventral stream which was not covered here, and future studies should focus on these regions to try to detect a representation of average size. What we observed, however, was that beta weights for density obtained from RSA regression became significant in the parietal regions during the size task, suggesting that texture processing mechanisms may be automatically activated during the average size task. This interpretation, however, has to remain speculative and future studies should investigate neural mechanisms relating texture, density and average size processing.

In conclusion, with this study using high-resolution, high-field fMRI we provide direct neuroscientific evidence for a processing mechanism dedicated to visual numerosity which is separable from the ones underlying the processing of non-numerical quantities from early stages of cortical processing on, and independently and progressively amplified across the dorsal visual stream when numerical information is explicitly processed. An important goal for the future will be to better understand what are the processing steps and transformations occurring at the different levels of the cortical hierarchy that characterize this specific sense of numerosity, for example by comparing fMRI data against computational models simulating the visual extraction of numerosity.

Methods

Subjects and MRI acquisition

Twenty healthy adults with normal or corrected vision (10 males and 10 females, mean age 24 years) participated in the study. The study was approved by the regional ethical committee (Hôpital de Bicêtre, France) and all participants gave written informed consent. Functional images were acquired on a SIEMENS MAGNETOM 7T scanner with head gradient insert (Gmax 80mT/m and slew rate 333T/m/s) and adapted 32-channel head coil (Nova Medical, Wilmington, MA, USA) as T2*-weighted fat-saturation echo-planar image (EPI) volumes with 1.3 mm isotropic voxels using a multi-band sequence (Moeller et al., 2010) (https://www.cmrr.umn.edu/multiband/, multi-band [MB] = 2, GRAPPA acceleration with [IPAT] = 2, partial Fourier [PF] = 7/8, matrix =120 x 150, repetition time [TR] = 2 s, echo time [TE] = 22 ms, echo spacing [ES] = 0.71 ms, flip angle [FA] = 68°, bandwidth [BW] = 1588 Hz/px, phase-encode direction left>>right). Calibration preparation was done using Gradient Recalled Echo (GRE) data. Sixty oblique slices covering the occipital, parietal and partially the frontal cortex were obtained in ascending interleaved order. Before the experimental runs two single volumes were acquired with the parameters listed above but with opposite phase encode direction to be used for distortion correction in the later analysis (see Image Processing and Data Analysis). T1-weighted anatomical images were acquired at 0.8 mm isotropic resolution using an MP2RAGE sequence (GRAPPA acceleration with [IPAT] = 3, partial Fourier [PF] = 6/8, matrix = 281 x 300, repetition time [TR] = 6 s, echo time [TE] = 2.92 ms, time of inversion [TI] 1/2= 800/2700 ms, flip angle [FA] 1/2 = 4°/5°, bandwidth [BW] = 240 Hz/px,). During scanning participants wore a radiofrequency absorbent jacket (Accusorb MRI, MWT Materials Inc., Passaic, NJ, USA) to minimize so-called “third-arm” or “shoulder” artifacts due to regions where the head gradient is unable to unambiguously spatially encode the image (Wald et al., 2005). Head movement was minimized by padding and tape. Visual stimuli were back-projected onto a translucent screen at the end of the scanner bore and viewed through a mirror attached to the head coil. Participants held two response buttons in their left and right hands.

Stimuli and procedure

During fMRI scanning participants were centrally presented with heterogeneous arrays of dots, half black, and half white, on a mid-gray background. The generated sets of dots were orthogonally varied in number, average item size and total field area for a total of 18 conditions: six, ten or seventeen dots were presented with either small, medium or large average item area (0.04, 0.07, 0.12 visual squares degree) and designed to fall within a small or large total field area (defined by a virtual circle of either about 5 or 7.5 visual degree diameter). Numbers and average item sizes were chosen to be perceptually equally discriminable based on a previous behavioral study (Castaldi et al., 2018). Total field areas were chosen so that arrays of dots could be sufficiently sparse (~1 dot/vd^2) to target the 'number regime' (Anobile et al., 2013, 2015).

Within each run participants performed two tasks in different blocks, as indicated by the written task instructions provided at the beginning of each block. Instructions were shown for 2 s and specified whether participants had to attend either to the number of dots (number task) or to the average item size of the dots (size task) in the array. Six seconds after the instruction a delayed comparison task started with brief presentation (500 ms) of a sample dot array stimulus. At each trial participants attended to the cued dimension of the sample stimulus and held this information in memory until the following trial was presented, knowing that a comparison response with the following trial may be required. After a variable ISI of 3.5 – 5.5 s, a second dot array was presented. If the color of the fixation point remained unchanged (green), no comparison was required and participants only had to update their memory with the new sample stimulus. If instead the fixation point changed color (turning to red 1 s before the stimulus presentation) participants had to compare the current stimulus (match stimulus) with the one held in memory and decide whether the current stimulus was larger or smaller (on the attended dimension) than the previous one. Response was provided by button press and after 5.5 s the next sample stimulus was presented and the whole procedure started again. Match stimuli were designed to be ~2 JNDs larger or smaller than the previously presented sample stimulus on the attended dimension, based on each participant's Weber fraction as measured in a behavioral test prior to the fMRI scanning, while the unattended dimension was the same as the previous sample stimulus.

Twenty trials were presented in each block: one trial for each one of the 18 sample stimulus conditions (3 numerosity x 3 sizes x 2 total field areas) and two match trials. The hands assigned to either the 'smaller' or 'larger' response were inverted in the middle of the scanning session, i.e. after the third run, and counterbalanced across subjects. Within the scanning session participants performed six runs of ~7 min and 44 s. Each run included four blocks where the two tasks alternated. The type of task with which the run started was balanced across runs and participants.

To measure their numerical and average size acuity, participants performed a behavioral test prior to the fMRI scanning. In different sessions participants were shown two consecutive centrally presented arrays of dots and were required to perform a discrimination task on the attended dimension (either numerosity or average item size) by pressing the left or the right arrow (to choose the first or the second stimulus respectively). The set of stimuli used included arrays of 5,7,9,11,15 and 20 dots (ratios 0.5, 0.7, 0.9, 1.1, 1.5 and 2 with respect to the reference of 10 dots) that could be displayed with the average dot areas of 0.05, 0.06, 0.08, 0.11, 0.15 and 0.2 visual square degrees (ratios 0.5, 0.6, 0.8, 1.1, 1.5 and 2 with respect to the reference of 0.1 visual square degrees). Dots were randomly drawn within two possible virtual circles of ~5.8 and 7.6 visual degrees diameter. Reference and test stimuli could appear either as first or as second stimulus. After task instructions and twelve practice trials, participants performed three sessions of one task and three sessions of the other, with counterbalanced order across subjects. For each task participants performed a total of 432 comparisons (6 numerosities x 6 average item sizes x 2 total field areas x 2 presentation order x 3 sessions). To quantify participants' precision in number and size judgments, we computed the JND for each task. The percentage of test trials with "greater than reference" responses was plotted against the log-transformed difference between test and reference and fitted with a cumulative Gaussian function using Psignifit toolbox (Schütt et al., 2016). The difference between the 50% and the 75% points yielded the JND.

Stimuli and paradigms were generated and presented under Matlab 9.0 using PsychToolbox routines (Brainard, 1997).

Image Processing and Data Analysis

EPI images were motion-corrected and co-registered to the first single band reference image using statistical parametric mapping software (SPM12, https://www.fil.ion.ucl.ac.uk/spm/software/spm12/). The single-band reference images of the two initial volumes acquired with opposite phase encode directions served to estimate a set of field coefficients using topup in FSL (https://fsl.fmrib.ox.ac.uk/fsl/fslwiki/FSL), which was subsequently used to apply distortion correction (apply_topup) to all EPI images. Cortical surface reconstruction and boundary based registration of single band reference images to each subject's cortical surface, as well as a minimal amount of surface constrained smoothing (FWHM = 1.5 mm) for noise reduction were performed in Freesurfer (https://surfer.nmr.mgh.harvard.edu/).

The preprocessed EPI images (in subjects' native space) were entered into a general linear model separately modeling the effects of the 36 sample conditions (3 numerosities x 3 average item sizes x 2 total field areas x 2 tasks, within each run the two repetitions for each condition were pooled together), the match stimulus separately for left and right hand and the written instructions at the beginning of the block as stick functions (using the default of 0 duration for events) convolved with the standard hemodynamic response function. The six motion parameters were included in the GLM as covariate of no interest. An AR(1) model was used to account for serial auto-correlation and low-frequency signal drifts were removed by a high-pass filter with a cutoff of 192 s. In each subject we contrasted the activation elicited by: all the sample stimuli during the number tasks against the implicit baseline (contrast name: 'Judge Number > Baseline'); all the sample stimuli during the size tasks against the implicit baseline (contrast name: 'Judge Size > Baseline'); all the sample stimuli during the number tasks against all the sample stimuli during the size tasks (contrast name: 'Judge Number > Judge Size). After creating the contrasts in each single subject's volume space, the contrast images were projected onto the surface with Freesurfer, aligned to fsaverage and smoothed with a 3-mm fwhm Gaussian kernel. The second-level group analysis was then performed in the surface space.

The beta estimates for the sample stimulus conditions from the first-level analysis (1 beta estimate per run and condition) were entered into pattern recognition analysis. In each subject we defined anatomical regions of interest (ROIs) derived from a surface based probabilistic atlas (Wang et al., 2015) where regions are defined based on retinotopy. ROIs for V1 to IPS5 were created on the Freesurfer surface and projected back into each subject's volume space. For each ROI we merged the left and right hemisphere. ROIs were further merged into three large ROIs corresponding to early (V1 to V3), intermediate (V3A, V3B and V7, also known as IPS0) and higher-level (IPS 1 to IPS5) areas. In addition we focused the analysis on individual regions: V1, V2, V3, V3AB (merging V3A and V3B), V7, IPS12 (merging IPS 1 and 2), IPS345 (merging IPS 3, 4 and 5). Within each one of these bilateral regions we selected on a subject-by-subject basis an equal number of 800 voxels that responded most strongly to the orthogonal contrast 'all sample stimuli > baseline' for pattern recognition analysis. To evaluate the degree of spatial consistency of the selected voxels across subjects we created an overlap map with Freesurfer (Fig 3B): single subjects' ROIs were aligned to fsaverage and the number of subjects for which a given location was included in their specific ROI was represented by a heat map (with yellow color meaning that a given location was selected in all subjects).

Pattern classification analysis was performed in scikit-learn (Pedregosa et al., 2011) using beta estimates after subtracting the voxel-wise mean across conditions by applying linear

667 support vector machines (SVM) with regularization parameter C=1. Classification analysis
668 was performed leaving patterns of one run out at each loop of the 6-fold cross-validation
669 cycle. This implies that classifiers were trained on five betas per condition and tested with the
670 left out beta images (one per condition). The classification accuracies obtained for each cycle
671 were then averaged together. Pairwise classification was performed for all pairs of
672 numerosities collapsing across the size and total field area dimensions, but keeping patterns
673 separated by task. Classification accuracy was then averaged across all pairs of
674 numerosities for each task. A one-sample t-test against the theoretical chance level of 50%
675 was performed to evaluate significance of discrimination. Repeated measures ANOVAs
676 where then performed on classification accuracies with ROI and task as factors.

677 For representational similarity analysis (RSA, Kriegeskorte, 2008; Kriegeskorte and Kievit,
678 2013) the GLM was performed concatenating the runs and obtaining one single beta per
679 condition, task and subject. Comparable to the procedure of the pattern classification
680 analysis, voxel-wise scaling was applied by subtracting the mean across conditions. Neural
681 representational dissimilarity matrices (neural RDMs) for each task and ROI were created by
682 computing the correlation distance (1 – the Pearson correlation across voxels) between
683 activity patterns associated with all possible pairs of conditions using CoSMoMVPA Toolbox
684 (Oosterhof et al., 2016). The neural RDMs were then entered in a multiple regression with
685 five predictors corresponding to matrices encoding the distance on a logarithmic scale for the
686 different quantitative dimensions defining the dot arrays: number, average item size, total
687 field area, total surface area and density. In the multiple regression analysis all distance
688 matrices were z-transformed before estimating the regression coefficients. The obtained beta
689 weights for each dimension and ROI were tested with one-sample t-tests against zero across
690 subjects. The effects of ROI, dimension and task were analyzed with repeated measures
691 ANOVAs.

692

693 Acknowledgements

694

695 This work was funded by the French National Research Agency (grant No ANR-14-CE13-
696 0020-01 to E. Eger). We thank F. De Martino and V. Kemper for advice on fMRI acquisition
697 parameters and procedures.

698

References

Anobile, G., Cicchini, G.M., and Burr, D. (2013). Separate mechanisms for perception of numerosity and density. Psychological Science 0956797613501520.

Anobile, G., Turi, M., Cicchini, G.M., and Burr, D. (2015). Mechanisms for perception of numerosity or texture-density are governed by crowding-like effects. Journal of Vision *15*, 4.

Anobile, G., Castaldi, E., Turi, M., Tinelli, F., and Burr, D. (2016a). Numerosity but not texture-density discrimination correlates with math ability in children. Developmental Psychology *52*, 1206–1216.

Anobile, G., Cicchini, G.M., and Burr, D. (2016b). Number As a Primary Perceptual Attribute: A Review. Perception *45*, 5–31.

Anobile, G., Arrighi, R., Castaldi, E., Grassi, E., Pedonese, L., M. Moscoso, P.A., and Burr, D. (2018). Spatial but Not Temporal Numerosity Thresholds Correlate With Formal Math Skills in Children. Developmental Psychology.

Arsalidou, M., and Taylor, M.J. (2011). Is 2+2=4? Meta-analyses of brain areas needed for numbers and calculations. NeuroImage *54*, 2382–2393.

Borghesani, V., de Hevia, M., Viarouge, A., Chagas, P., Eger, E., and Piazza, M. (2018). Processing number and length in the parietal cortex: Sharing resources, not a common code. Cortex.

Brainard, D.H. (1997). The psychophysics toolbox. Spatial Vision *10*, 433–436.

Bulthé, J., De Smedt, B., and Op de Beeck, H.P. (2014). Format-dependent representations of symbolic and non-symbolic numbers in the human cortex as revealed by multi-voxel pattern analyses. NeuroImage *87*, 311–322.

Bulthé, J., De Smedt, B., and Op de Beeck, H.P. (2015). Visual Number Beats Abstract Numerical Magnitude: Format-dependent Representation of Arabic Digits and Dot Patterns in Human Parietal Cortex. Journal of Cognitive Neuroscience *27*, 1376–1387.

Burr, D., and Ross, J. (2008). A Visual Sense of Number. Current Biology *18*, 425–428.

Cant, J.S., and Xu, Y. (2012). Object Ensemble Processing in Human Anterior-Medial Ventral Visual Cortex. Journal of Neuroscience *32*, 7685–7700.

Cantlon, J.F. (2012). Math, monkeys, and the developing brain. Proceedings of the National Academy of Sciences *109*, 10725–10732.

Carrasco, M. (2011). Visual attention: The past 25 years. Vision Research *51*, 1484–1525.

Castaldi, E., Aagten-Murphy, D., Tosetti, M., Burr, D., and Morrone, M.C. (2016). Effects of adaptation on numerosity decoding in the human brain. NeuroImage.

Castaldi, E., Mirassou, A., Dehaene, S., Piazza, M., and Eger, E. (2018). Asymmetrical interference between number and item size perception provides evidence for a domain specific impairment in dyscalculia. PLOS ONE *13*, e0209256.

734 Cavdaroglu, S., and Knops, A. (2018). Evidence for a Posterior Parietal Cortex Contribution to Spatial
735 but not Temporal Numerosity Perception. Cerebral Cortex.

736 Cavina-Pratesi, C., Kentridge, R.W., Heywood, C.A., and Milner, A.D. (2010). Separate Channels for
737 Processing Form, Texture, and Color: Evidence from fMRI Adaptation and Visual Object Agnosia.
738 Cerebral Cortex *20*, 2319–2332.

739 Chen, Q., and Li, J. (2014). Association between individual differences in non-symbolic number acuity
740 and math performance: A meta-analysis. Acta Psychologica *148*, 163–172.

741 Cicchini, G.M., Anobile, G., and Burr, D. (2016). Spontaneous perception of numerosity in humans.
742 Nature Communications *7*, 12536.

743 Dakin, S.C., Tibber, M.S., Greenwood, J.A., Kingdom, F.A.A., and Morgan, M.J. (2011). A common
744 visual metric for approximate number and density. Proceedings of the National Academy of Sciences
745 *108*, 19552–19557.

746 David, S.V., Hayden, B.Y., Mazer, J.A., and Gallant, J.L. (2008). Attention to Stimulus Features Shifts
747 Spectral Tuning of V4 Neurons during Natural Vision. Neuron *59*, 509–521.

748 De Smedt, B., Noël, M., Gilmore, C., and Ansari, D. (2013). How do symbolic and non-symbolic
749 numerical magnitude processing skills relate to individual differences in children's mathematical
750 skills? A review of evidence from brain and behavior. Trends in Neuroscience and Education *2*, 48–55.

751 Dehaene, S. (1997). The number sense: how the mind creates mathematics (New York: Oxford
752 University Press).

753 Dehaene, S., and Changeux, J. (1993). Development of Elementary Numerical Abilities: A Neuronal
754 Model. Journal of Cognitive Neuroscience *5*, 390–407.

755 DeWind, N.K., Adams, G.K., Platt, M.L., and Brannon, E.M. (2015). Modeling the approximate number
756 system to quantify the contribution of visual stimulus features. Cognition *142*, 247–265.

757 DeWind, N.K., Park, J., Woldorff, M.G., and Brannon, E.M. (2018). Numerical encoding in early visual
758 cortex. Cortex.

759 Dormal, V., and Pesenti, M. (2009). Common and specific contributions of the intraparietal sulci to
760 numerosity and length processing. Human Brain Mapping *30*, 2466–2476.

761 Eger, E. (2016). Neuronal foundations of human numerical representations. In Progress in Brain
762 Research, (Elsevier), pp. 1–27.

763 Eger, E., Michel, V., Thirion, B., Amadon, A., Dehaene, S., and Kleinschmidt, A. (2009). Deciphering
764 Cortical Number Coding from Human Brain Activity Patterns. Current Biology *19*, 1608–1615.

765 Eger, E., Pinel, P., Dehaene, S., and Kleinschmidt, A. (2015). Spatially Invariant Coding of Numerical
766 Information in Functionally Defined Subregions of Human Parietal Cortex. Cerebral Cortex *25*, 1319–
767 1329.

768 Ester, E.F., Sutterer, D.W., Serences, J.T., and Awh, E. (2016). Feature-Selective Attentional
769 Modulations in Human Frontoparietal Cortex. Journal of Neuroscience *36*, 8188–8199.

770 Fias, W. (2016). Neurocognitive Components of Mathematical Skills and Dyscalculia. In Development
771 of Mathematical Cognition, (Elsevier), pp. 195–217.

772 Fischl, B. (2004). Automatically Parcellating the Human Cerebral Cortex. Cerebral Cortex *14*, 11–22.

773 Fornaciai, M., and Park, J. (2017). Distinct Neural Signatures for Very Small and Very Large
774 Numerosities. Frontiers in Human Neuroscience *11*.

775 Fornaciai, M., and Park, J. (2018). Neural Sensitivity to Numerosity in Early Visual Cortex Is Not
776 Sufficient for the Representation of Numerical Magnitude. Journal of Cognitive Neuroscience 1–15.

777 Fornaciai, M., Brannon, E.M., Woldorff, M.G., and Park, J. (2017). Numerosity processing in early
778 visual cortex. NeuroImage *157*, 429–438.

779 Freedman, D.J., and Assad, J.A. (2009). Distinct Encoding of Spatial and Nonspatial Visual Information
780 in Parietal Cortex. Journal of Neuroscience *29*, 5671–5680.

781 Gebuis, T., and Reynvoet, B. (2012). The interplay between nonsymbolic number and its continuous
782 visual properties. Journal of Experimental Psychology: General *141*, 642–648.

783 Gebuis, T., Gevers, W., and Kadosh, R.C. (2014). Topographic representation of high-level cognition:
784 numerosity or sensory processing? Trends in Cognitive Sciences *18*, 1–3.

785 Gottlieb, J. (2007). From Thought to Action: The Parietal Cortex as a Bridge between Perception,
786 Action, and Cognition. Neuron *53*, 9–16.

787 Halberda, J., Mazzocco, M.M.M., and Feigenson, L. (2008). Individual differences in non-verbal
788 number acuity correlate with maths achievement. Nature *455*, 665–668.

789 Harvey, B.M., and Dumoulin, S.O. (2017a). A network of topographic numerosity maps in human
790 association cortex. Nature Human Behaviour *1*, 0036.

791 Harvey, B.M., and Dumoulin, S.O. (2017b). Can responses to basic non-numerical visual features
792 explain neural numerosity responses? NeuroImage *149*, 200–209.

793 Harvey, B.M., Klein, B.P., Petridou, N., and Dumoulin, S.O. (2013). Topographic Representation of
794 Numerosity in the Human Parietal Cortex. Science *341*, 1123–1126.

795 Harvey, B.M., Fracasso, A., Petridou, N., and Dumoulin, S.O. (2015). Topographic representations of
796 object size and relationships with numerosity reveal generalized quantity processing in human
797 parietal cortex. Proceedings of the National Academy of Sciences *112*, 13525–13530.

798 de Hevia, M.D., Castaldi, E., Streri, A., Eger, E., and Izard, V. (2017). Perceiving numerosity from birth.
799 Behavioral and Brain Sciences,40.

800 Hyde, D.C., and Spelke, E.S. (2011). Neural signatures of number processing in human infants:
801 evidence for two core systems underlying numerical cognition: Neural signatures of number in
802 infants. Developmental Science *14*, 360–371.

803 Ibos, G., and Freedman, D.J. (2014). Dynamic Integration of Task-Relevant Visual Features in
804 Posterior Parietal Cortex. Neuron *83*, 1468–1480.

805 Im, H.Y., and Halberda, J. (2013). The effects of sampling and internal noise on the representation of
806 ensemble average size. Attention, Perception, & Psychophysics *75*, 278–286.

807 Itti, L., and Koch, C. (2001). Computational modelling of visual attention. Nature Reviews
808 Neuroscience *2*, 194–203.

809 Iuculano, T., and Menon, V. (2018). Development of Mathematical Reasoning. In Stevens' Handbook
810 of Experimental Psychology and Cognitive Neuroscience, p.

811 Izard, V., Dehaene-Lambertz, G., and Dehaene, S. (2008). Distinct cerebral pathways for object
812 identity and number in human infants. PLoS Biology *6*, e11.

813 Jehee, J.F.M., Brady, D.K., and Tong, F. (2011). Attention Improves Encoding of Task-Relevant
814 Features in the Human Visual Cortex. Journal of Neuroscience *31*, 8210–8219.

815 Kamitani, Y., and Tong, F. (2005). Decoding the visual and subjective contents of the human brain.
816 Nature Neuroscience *8*, 679–685.

817 Kamitani, Y., and Tong, F. (2006). Decoding Seen and Attended Motion Directions from Activity in the
818 Human Visual Cortex. Current Biology *16*, 1096–1102.

819 Kastner, S., Chen, Q., Jeong, S.K., and Mruczek, R.E.B. (2017). A brief comparative review of primate
820 posterior parietal cortex: A novel hypothesis on the human toolmaker. Neuropsychologia *105*, 123–
821 134.

822 Kourtzi, Z., and Grill-Spector, K. (2005). fMRI Adaptation: A Tool for Studying Visual Representations
823 in the Primate Brain. In Fitting the Mind to the WorldAdaptation and After-Effects in High-Level
824 Vision, (Clifford Colin W. G., Rhodes Gillian), p.

825 Kriegeskorte, N. (2008). Representational similarity analysis – connecting the branches of systems
826 neuroscience. Frontiers in Systems Neuroscience.

827 Kriegeskorte, N., and Kievit, R.A. (2013). Representational geometry: integrating cognition,
828 computation, and the brain. Trends in Cognitive Sciences *17*, 401–412.

829 Lasne, G., Piazza, M., Dehaene, S., Kleinschmidt, A., and Eger, E. (2018). Discriminability of
830 numerosity-evoked fMRI activity patterns in human intra-parietal cortex reflects behavioral
831 numerical acuity. Cortex.

832 Leibovich, T., Katzin, N., Harel, M., and Henik, A. (2016). From 'sense of number'to 'sense of
833 magnitude'–The role of continuous magnitudes in numerical cognition. Behavioral and Brain Sciences
834 1–62.

835 Libertus, M.E., Feigenson, L., and Halberda, J. (2011). Preschool acuity of the approximate number
836 system correlates with school math ability: Approximate number system and math abilities.
837 Developmental Science *14*, 1292–1300.

838 Libertus, M.E., Feigenson, L., and Halberda, J. (2013). Is approximate number precision a stable
839 predictor of math ability? Learning and Individual Differences *25*, 126–133.

840 Liu, T., Hospadaruk, L., Zhu, D.C., and Gardner, J.L. (2011). Feature-Specific Attentional Priority
841 Signals in Human Cortex. Journal of Neuroscience *31*, 4484–4495.

Martinez-Trujillo, J.C., and Treue, S. (2004). Feature-Based Attention Increases the Selectivity of Population Responses in Primate Visual Cortex. Current Biology *14*, 744–751.

McAdams, C.J., and Maunsell, J.H.R. (2000). Attention to Both Space and Feature Modulates Neuronal Responses in Macaque Area V4. Journal of Neurophysiology *83*, 1751–1755.

Moeller, S., Yacoub, E., Olman, C.A., Auerbach, E., Strupp, J., Harel, N., and Uğurbil, K. (2010). Multiband multislice GE-EPI at 7 tesla, with 16-fold acceleration using partial parallel imaging with application to high spatial and temporal whole-brain fMRI. Magnetic Resonance in Medicine *63*, 1144–1153.

Morgan, M.J., Raphael, S., Tibber, M.S., and Dakin, S.C. (2014). A texture-processing model of the "visual sense of number." Proceedings of the Royal Society B: Biological Sciences *281*, 20141137–20141137.

Nieder, A. (2016). The neuronal code for number. Nature Reviews Neuroscience *17*, 366–382.

Nieder, A., and Miller, E.K. (2004). A parieto-frontal network for visual numerical information in the monkey. Proceedings of the National Academy of Sciences of the United States of America *101*, 7457–7462.

Nieder, A., Freedman, D.J., and Miller, E.K. (2002). Representation of the quantity of visual items in the primate prefrontal cortex. Science *297*, 1708–1711.

Norman, K.A., Polyn, S.M., Detre, G.J., and Haxby, J.V. (2006). Beyond mind-reading: multi-voxel pattern analysis of fMRI data. Trends in Cognitive Sciences *10*, 424–430.

Oosterhof, N.N., Connolly, A.C., and Haxby, J.V. (2016). CoSMoMVPA: Multi-Modal Multivariate Pattern Analysis of Neuroimaging Data in Matlab/GNU Octave. Frontiers in Neuroinformatics *10*.

Park, J., DeWind, N.K., Woldorff, M.G., and Brannon, E.M. (2015). Rapid and Direct Encoding of Numerosity in the Visual Stream. Cerebral Cortex bhv017.

Pedregosa, F., Varoquaux, G., Gramfort, A., Michel, V., Thirion, B., Grisel, O., Blondel, M., Prettenhofer, P., Weiss, R., Dubourg, V., et al. (2011). Scikit-learn: Machine Learning in Python. 7.

Piazza, M., and Eger, E. (2016). Neural foundations and functional specificity of number representations. Neuropsychologia *83*, 257–273.

Piazza, M., Izard, V., Pinel, P., Le Bihan, D., and Dehaene, S. (2004). Tuning curves for approximate numerosity in the human intraparietal sulcus. Neuron *44*, 547–555.

Piazza, M., Facoetti, A., Trussardi, A.N., Berteletti, I., Conte, S., Lucangeli, D., Dehaene, S., and Zorzi, M. (2010). Developmental trajectory of number acuity reveals a severe impairment in developmental dyscalculia. Cognition *116*, 33–41.

Piazza, M., Pica, P., Izard, V., Spelke, E., and Dehaene, S. (2013). Education Enhances the Acuity of the Nonverbal Approximate Number System. Psychological Science *24*, 1037–1043.

Pinel, P., Piazza, M., Le Bihan, D., and Dehaene, S. (2004). Distributed and Overlapping Cerebral Representations of Number, Size, and Luminance during Comparative Judgments. Neuron *41*, 983–993.

879 Reynolds, J.H., Pasternak, T., and Desimone, R. (2000). Attention Increases Sensitivity of V4 Neurons.
880 Neuron *26*, 703–714.

881 Roitman, J., Brannon, E.M., and Platt, M.L. (2007). Monotonic Coding of Numerosity in Macaque
882 Lateral Intraparietal Area. PLoS Biology *5*, e208.

883 Ross, J. (2010). Vision senses number directly. Journal of Vision *10*, 1–8.

884 Sapountzis, P., Paneri, S., and Gregoriou, G.G. (2018). Distinct roles of prefrontal and parietal areas in
885 the encoding of attentional priority. Proceedings of the National Academy of Sciences *115*, E8755–
886 E8764.

887 Schütt, H.H., Harmeling, S., Macke, J.H., and Wichmann, F.A. (2016). Painfree and accurate Bayesian
888 estimation of psychometric functions for (potentially) overdispersed data. Vision Research *122*, 105–
889 123.

890 Serences, J.T., and Boynton, G.M. (2007). Feature-Based Attentional Modulations in the Absence of
891 Direct Visual Stimulation. Neuron *55*, 301–312.

892 Sokolowski, H.M., Fias, W., Bosah Ononye, C., and Ansari, D. (2017). Are numbers grounded in a
893 general magnitude processing system? A functional neuroimaging meta-analysis. Neuropsychologia.

894 Stoianov, I., and Zorzi, M. (2012). Emergence of a “visual number sense” in hierarchical generative
895 models. Nature Neuroscience *15*, 194–196.

896 Thompson, K., and Bichot, N. (2005). A visual salience map in the primate frontal eye field. Prog Brain
897 Res. 147:251-62.

898 Tong, F., and Pratte, M.S. (2012). Decoding Patterns of Human Brain Activity. Annual Review of
899 Psychology *63*, 483–509.

900 Toth, L.J., and Assad, J.A. (2002). Dynamic coding of behaviourally relevant stimuli in parietal cortex.
901 Nature *415*, 165–168.

902 Treue, S., and Trujillo, J.C.M. (1999). Feature-based attention influences motion processing gain in
903 macaque visual cortex. Nature *399*, 575–579.

904 Verguts, T., and Fias, W. (2004). Representation of Number in Animals and Humans: A Neural Model.
905 Journal of Cognitive Neuroscience *16*, 1493–1504.

906 Viswanathan, P., and Nieder, A. (2015). Differential Impact of Behavioral Relevance on Quantity
907 Coding in Primate Frontal and Parietal Neurons. Current Biology *25*, 1259–1269.

908 Wald, L.L., Wiggins, G.C., Potthast, A., Wiggins, C.J., and Triantafyllou, C. (2005). Design
909 Considerations and Coil Comparisons for 7 Tesla Brain Imaging. Proc. Intl. Soc. Mag. Reson. Med. *13*,
910 1.

911 Wang, L., Mruczek, R.E.B., Arcaro, M.J., and Kastner, S. (2015). Probabilistic Maps of Visual
912 Topography in Human Cortex. Cerebral Cortex *25*, 3911–3931.

913

Figures

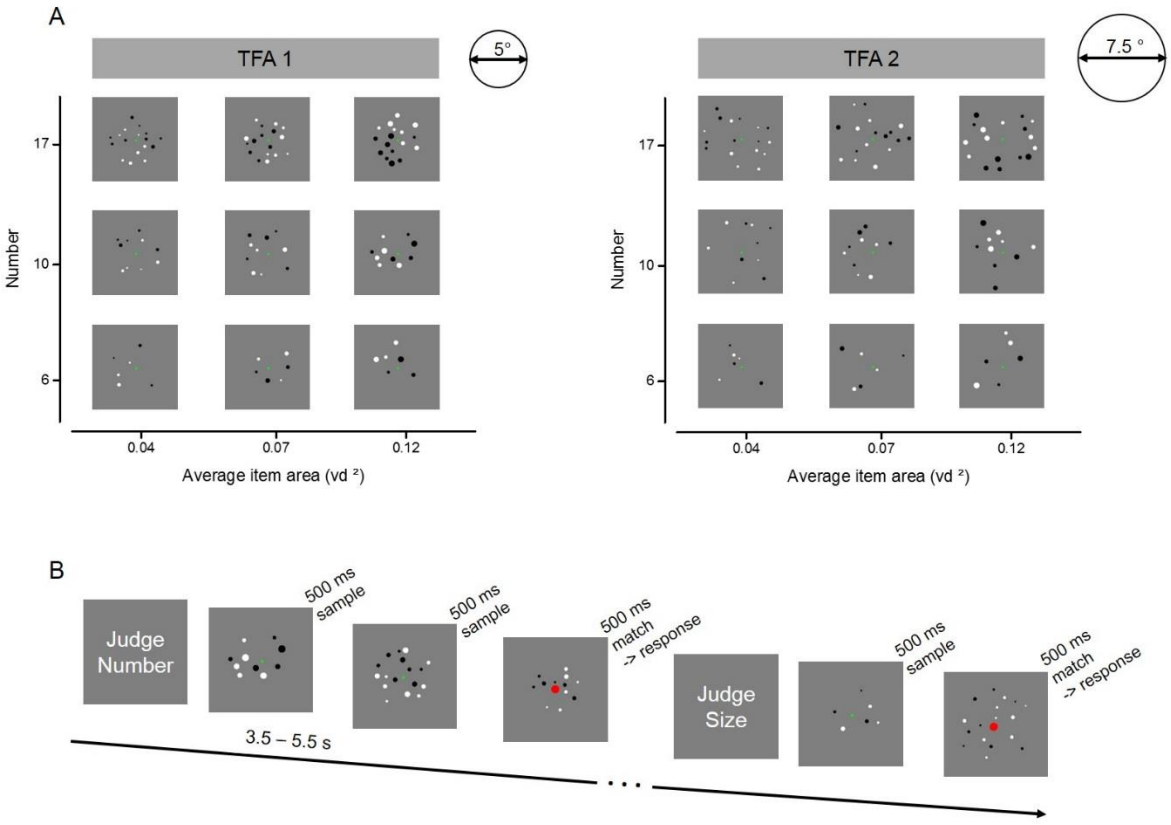

Fig 1 Stimulus set and design for the fMRI experiment

(A) Example of the full set of stimulus conditions. Arrays of six, ten or seventeen dots were created with three average item areas (0.04, 0.07 and 0.12 visual degree^2) and displayed within two total field areas, enclosed by imaginary circles of 5° (TFA 1) and 7.5° (TFA 2) diameter. (B) Illustration of the trials' temporal presentation and paradigm during scanning. At the beginning of each block, written instructions informed participants about the dimension to attend: either the numerosity or the average size of the dots arrays. Participants were instructed to keep in memory the relevant dimension of each sample trial until the following trial was shown (after a variable time interval of 3.5 - 5.5 s). The color of the fixation point in the upcoming trial provided further instruction: if it remained green, participants had to update their memory with the new stimulus (new sample trial), while if it turned red, participants had to compare the current stimulus (match trial) with the one kept in memory, and to indicate by button press whether the match stimulus was larger or smaller than the sample on the attended dimension. After the response a new sample stimulus appeared after at least 8 seconds. FMRI analyses focused on activity evoked by sample stimuli only.

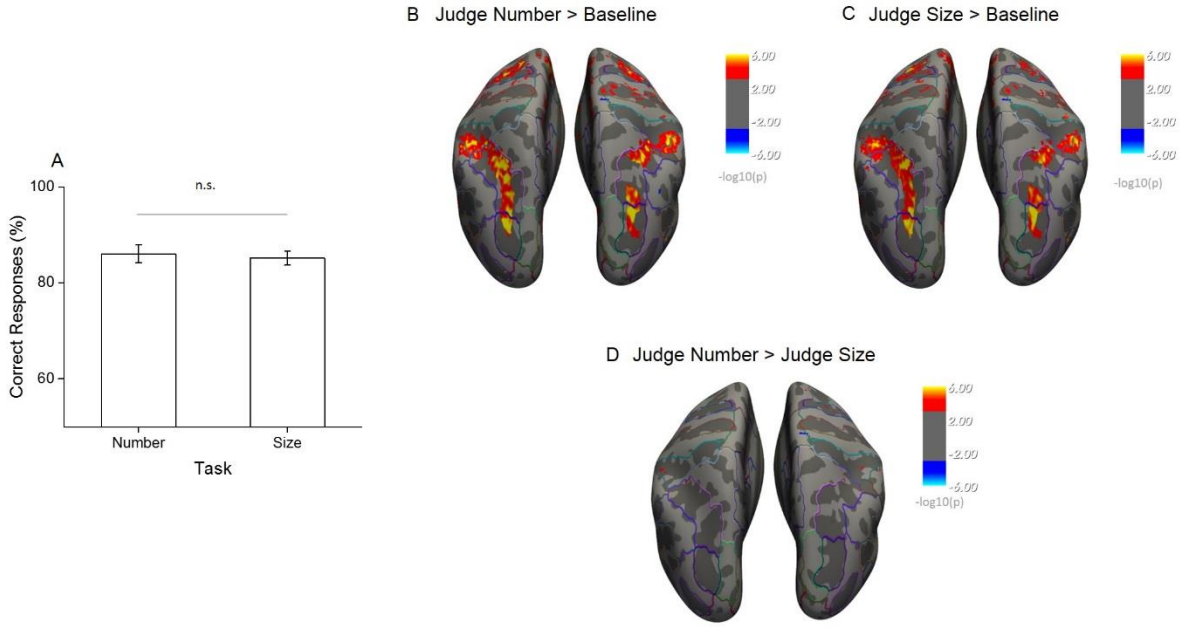

Fig 2 Behavioral performance during scanning and univariate effects of task

(A) The percentage of correct responses to match stimuli for the two tasks performed during scanning shows that task difficulty was successfully matched. (B-D) Statistical results obtained from the surface based group analysis (n=20). The maps show the activation elicited for all sample trials during the number task (B) and the size task (C) when contrasted against the implicit baseline and against each other (D). Activation maps are thresholded at $p<0.001$, uncorrected for multiple comparison, and displayed on Freesurfer's fsaverage surface with outlines identifying the major sulci and gyri based on the Destrieux Atlas.

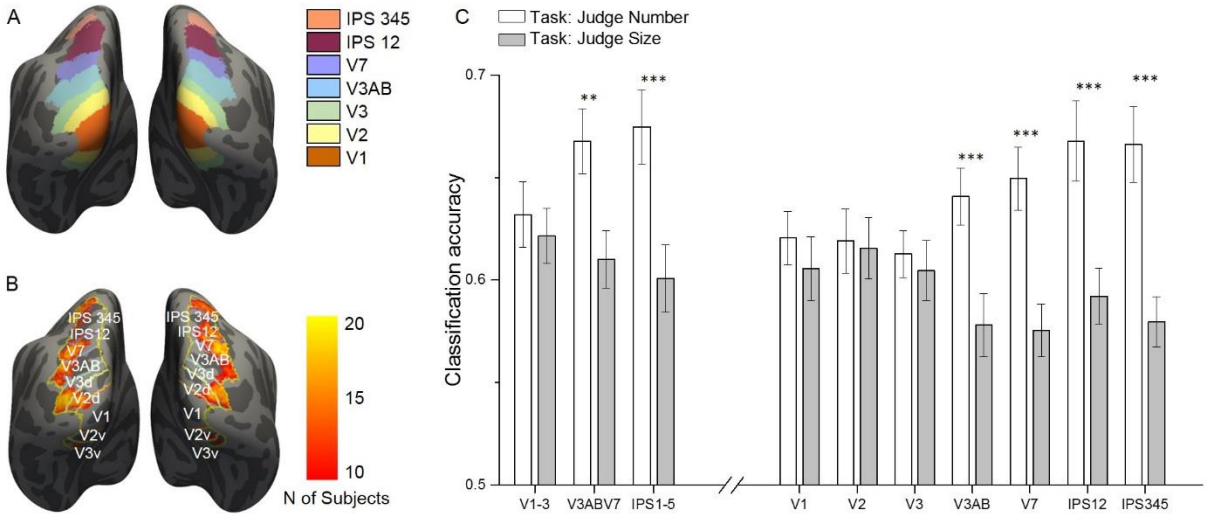

Fig 3 ROI localization and results of multivariate classification for discrimination between numerosities as a function of the task

(A) Color-coded ROIs defined by the probabilistic atlas are shown on the inflated brain template. (B) Across-subject overlap map of the most activated voxels in the contrast all sample>baseline. For each subject the most activated voxels were selected from each ROI (outlines) and hemisphere and the color map shows the number of subjects for which a given location was selected. (C) Sample numerosities could be classified significantly above chance across all the combined (left side) and individual (right side) ROIs, both during the number (white bars) and size (gray bars) task. The classification performance is strongly modulated by task only in the intermediate and higher-level ROIs, starting from V3AB on, but not in the early areas (V1, V2 and V3). Results show mean classification accuracy across subjects (n=20) ± standard error of the mean (SEM).

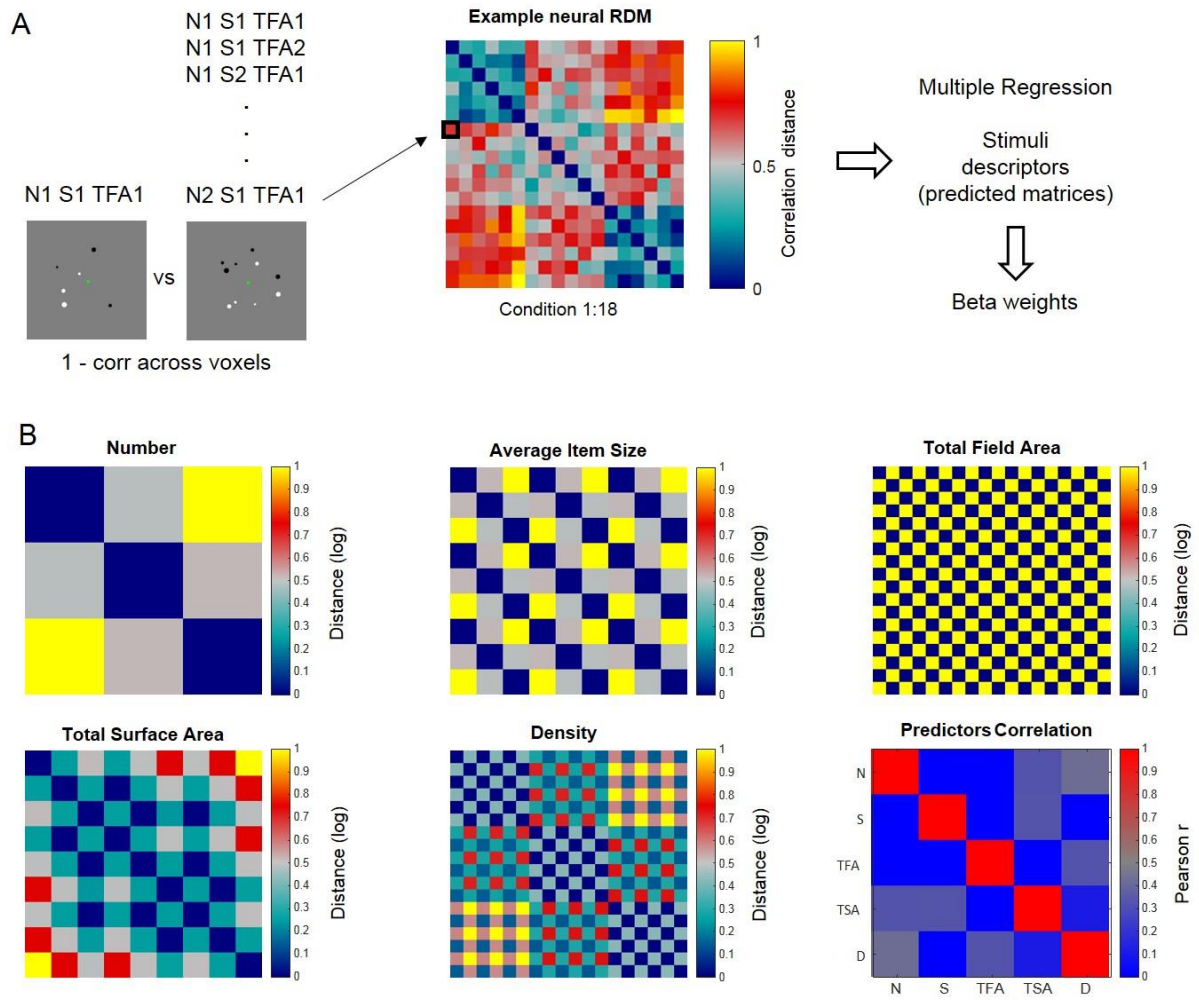

Fig 4 Schematic Illustration of Representational Similarity Analysis

Neural representational dissimilarity matrices (RDM) derived from fMRI were entered in a multiple regression where predictors corresponded to five matrices describing the dissimilarities across stimulus conditions along numerical and non-numerical dimensions. (A) Example neural RDM, quantifying the correlation distance (1 – Pearson correlation) between the patterns of activity elicited by all possible pairs of stimulus conditions across voxels within a given ROI (matrix scaled between 0 and 1 for visualization purposes). Each cell represents the correlation distance between activity patterns associated with a given pair of stimulus conditions (relatively lower values indicate more similar, and higher values more dissimilar patterns, respectively). (B) The five dissimilarity matrices used as predictors in the multiple regression analysis represent the logarithmic distance between pairs of stimuli in terms of number, average item size, total field area, total surface area and density (all matrices scaled between 0 and 1 for visualization purposes). The correlation across these five predicted matrices is shown in the 'predictor correlation' matrix. The orthogonal combination of number (N), average item size (S) and total field area (TFA) levels in our design ensured that number was also partially de-correlated from total surface area (TSA) and density (D).

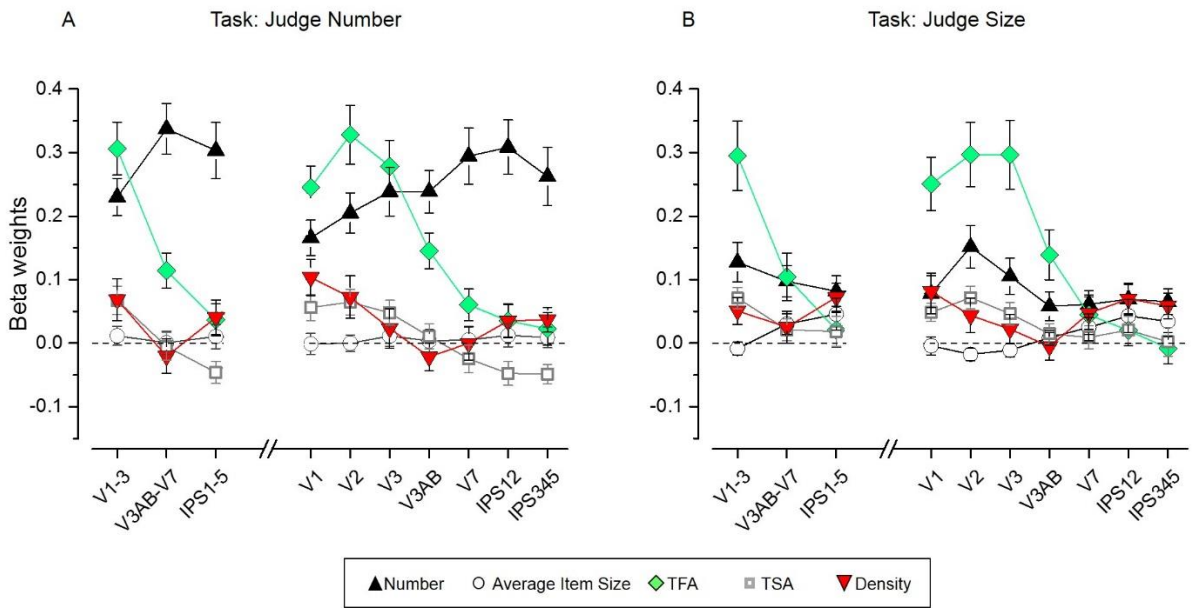

Fig 5 Results of the Representational Similarity Analysis

Beta weights obtained from the RSA multiple regression analysis for number (black triangles), average item size (circles), total field area (TFA, diamonds), total surface area (TSA, squares) and density (red triangles) for the number (A) and size (B) task. While the fMRI pattern dissimilarity in early visual areas reflected contributions of multiple properties (TFA, density, TSA, but also number on top of these), when attending to number (A) the dissimilarity matrix for number increasingly better explained the fMRI pattern dissimilarity when progressing towards higher areas of the dorsal visual stream, where the contribution of non-numerical dimensions was smaller. The dissimilarity matrix for number however, contributed much less to explain neural dissimilarity in mid- and higher-level ROIs during the size task (B). The contribution of the non-numerical dissimilarity matrices remained mostly unaffected in most of the ROIs, with only a slightly enhanced contribution of the dissimilarity matrix for density which significantly contributed to explain the neural RDMs in higher areas during the size judgments. Data points show mean beta weights across subjects (n=20) ± standard error of the mean (SEM). P-values testing the significance of the beta coefficients for each dimension and ROI are reported in Table 1 in Supplementary Material.

Supplementary Material

Tables

Task: Judge Number										
Stat\ROI	V1-3	V3AB-V7	IPS 1-5	V1	V2	V3	V3AB	V7	IPS12	IPS345
t-value	39.38	42.13	37.00	47.64	39.36	53.33	45.95	42.17	34.12	35.76
Dof	19	19	19	19	19	19	19	19	19	19
p-value	<.0005	<.0005	<.0005	<.0005	<.0005	<.0005	<.0005	<.0005	<.0005	<.0005
Task: Judge Size										
Stat\ROI	V1-3	V3AB-V7	IPS 1-5	V1	V2	V3	V3AB	V7	IPS12	IPS345
t-value	46.75	43.47	36.38	38.81	41.11	41.21	37.43	45.20	43.56	47.82
Dof	19	19	19	19	19	19	19	19	19	19
p-value	<.0005	<.0005	<.0005	<.0005	<.0005	<.0005	<.0005	<.0005	<.0005	<.0005

Table 1 Statistical results for the performance of the classifiers trained to discriminate between different numerosities.

The table reports t-values, degrees of freedom (Dof) and p-values of the two-tailed t-tests against zero used to evaluate the accuracies of number classification for every ROI and task.

Task: Judge Number										
Dim\ROI	V1-3	V3AB-V7	IPS 1-5	V1	V2	V3	V3AB	V7	IPS12	IPS345
N	<.0005	<.0005	<.0005	<.0005	<.0005	<.0005	<.0005	<.0005	<.0005	<.0005
S	.447	.972	.587	.946	.996	.495	.836	.818	.500	.587
TFA	<.0005	.001	.157	<.0005	<.0005	<.0005	<.0005	.025	.185	.392
TSA	.007	.815	.016	.014	.005	.026	.580	.271	.021	.005
D	.052	.456	.151	.002	.043	.464	.339	.998	.200	.075
Task: Judge Size										
Dim\ROI	V1-3	V3AB-V7	IPS 1-5	V1	V2	V3	V3AB	V7	IPS12	IPS345
N	.001	.001	.003	.024	<.0005	.001	.020	.010	.013	.005
S	.405	.086	.083	.777	.085	.339	.459	.243	.119	.155
TFA	<.0005	.012	.445	<.0005	<.0005	<.0005	.002	.170	.419	.747
TSA	<.0005	.238	.439	.003	.001	.017	.361	.622	.352	.921
D	.025	.328	.004	.004	.127	.348	.821	.083	.007	.009

Table 2 Statistical results for beta weights obtained from the RSA multiple regression.

The table shows p-values of two-tailed t-tests against zero across subjects for every ROI and dimension (N: number, S: average item size, TFA: total field area, TSA: total surface area, D: density) for the number (upper table) and size (lower table) tasks.